Phys. Status Solidi B **249**, No. 3, 435–447 (2012) / **DOI** 10.1002/pssb.201147402

physica status solidi b
www.pss-b.com
basic solid state physics

Editor's Choice

Coherent manipulation of quadrupole biexcitons in cuprous oxide by 2D femtosecond spectroscopy

Oleksiy Roslyak[*,1,3], Upali Aparajita[1,2], Joseph L. Birman[2], and Shaul Mukamel[3]

[1] Physics Department, Hunter College, CUNY, 695 Park Avenue, New York, NY 10065, USA
[2] Physics Department, The City College of New York, 160 Convent Avenue, New York, NY 10031, USA
[3] Chemistry Department, University of California, Irvine-Irvine, CA 92697, USA

Received 9 August 2011, revised 6 November 2011, accepted 7 November 2011
Published online 21 December 2011

Keywords collective effects, excited states, intrinsic properties of excitons, optical absorption spectra

[*] Corresponding author: e-mail avroslyak@gmail.com, Phone: +1 718 413 6495, Fax: +1 212 772 5390

We propose using coherent optical spectroscopy to study and control optically-forbidden (dark) biexciton states in crystals of cuprous oxide. These states are revealed in the correlation spectra cross resonances due to coherence with the quadrupole allowed 1*S* exciton manifold. The signal is obtained by means of sum-over-state formalism and comparing equations of motion for the weakly interacting quadrupole excitons with their analogue of non-interacting quasiparticles. The dephasing mechanisms include rapid Auger relaxation of biexcitons which allegedly impedes the Bose–Einstein condensation of quadrupole excitons. An interesting effect attributed to the deviation of the quadrupole excitons from the *ortho–para* excitons picture is that the positions of the biexciton resonances are defined by the energy splitting between $\Gamma^{+}_{5;yz}$ and $\Gamma^{+}_{5;xz}$ excitons and can be tuned by an external perturbation. Possible quantum computing and lasing applications of the quadrupole induced chirality effects of the excitons and biexcitons, and coherence between exciton/biexciton manifolds are discussed.

1 Introduction Cuprous oxide is a good candidate for observing Bose–Einstein condensation (BEC) of excitons for several reasons. The relatively large effective mass of the electrons in the conduction band (m_e) and holes in the valence band (m_h) results in a small exciton radius ($a_X = 5.1$ Å), according to Kavoulakis [1] who considered "central cell corrections." Equal parity of the conduction and valence band states produces dipole-forbidden, quadrupole-allowed 1*S* exciton which is characterized by a long radiative life-time depending on a dominating dephasing mechanism and varies from ns to ps. At low exciton density the measured life-time (≈1.7 ns) is determined by phonon-assisted non-radiative transitions between *ortho* ($J = 1$) and optically forbidden *para* ($J = 0$) excitons separated by 12 meV due to spin–orbit interaction. Thanks to the small radius, the exciton gas saturation density $n_s = 10^{20}\,\mathrm{cm}^{-3}$ is much higher than the critical density $n_c = 10^{17}\,\mathrm{cm}^{-3}$ needed for the quadrupole exciton BEC at $T = 2$ K.

Unfortunately, BEC turned out to be an elusive goal due to a strong recombination process that becomes effective at gas densities above $\approx 10^{14}\,\mathrm{cm}^{-3}$. Usually, this undesirable effect is attributed to an exciton Auger process, i.e., upon collision one of the excitons recombines and contributes its band-gap energy to the kinetic energy of the remaining electron and hole [2–6]. But there is a substantial discrepancy between theory and time-resolved photoluminescence (which measures the decay of exciton number following short optical pulse excitation). The calculated direct ($2 \times 10^{-21}\,\mathrm{cm}^3$/ns at a temperature of 70 K) [7] and phonon-assisted Auger decay rates ($3 \times 10^{-22}\,\mathrm{cm}^3$/ns) [8, 9] are orders of magnitude smaller than measured decay rate ($10^{-16}\,\mathrm{cm}^3$/ns) [3]. Moreover, conventional Auger theory predicts a linear increase of the Auger rate with temperature, whereas experiment [7] shows an inverse temperature dependence.

These discrepancies suggest that another mechanism may be responsible for enhancement of the Auger decay rate. Even though biexcitons have not been directly observed, it was proposed that possible formation of bound biexciton (exciton molecule) might be responsible for the rapid decay [10]. Auger decay of a biexciton produces a hot electron–hole pair with the energy gained from non-radiative

recombination of the other electron–hole pair. This heating of the lattice and exciton gas could explain the difficulties in achieving BEC of excitons in cuprous oxide, provided that we have an unambiguous proof of the biexciton formation. Be that as it may, in this "forbidden-gap" material the lowest biexciton states are optically forbidden and may not be detected by either direct or phonon-assisted photoluminescence or absorption. Non-linear optical processes are sensitive to the interactions between quasiparticles and provide direct information on processes that are inaccessible with linear spectroscopic techniques. Recently some novel 2D correlation spectroscopic techniques have been applied to study exciton and biexciton formation, their dynamics and transport in bulk semiconductors, quantum wells and quantum dots [11–14]. In these time domain experiments, a train of well separated optical pulses excites the sample and the generated $\chi^{(3)}$ signal is heterodyne detected in one of the possible phase matching conditions.

In this work, we propose to use excited state emission into $\mathbf{k}_{III} = \mathbf{k}_1 + \mathbf{k}_2 - \mathbf{k}_3$ direction to establish the existence and reveal key properties of the biexcitons in cuprous oxide. Assuming the initial exciton/biexciton density distribution at the given temperature, we shall determine the biexciton binding energy and Auger lifetime (scattering coefficient). There are two main approaches to calculate the signal. One is based on non-linear exciton equations (NEE) and the needed formalism can be found in Ref. [28]. The signal is given in terms of single exciton Green's function and is proportional to the exciton scattering matrix. Finding the latter proved to be computationally extensive even for much simpler systems of the molecular assembly. To interpret the results of the simulation one usually needs the sum-over-states (SOS) form of the signal [21]. The SOS formalism utilizes the non-interacting quasiparticle representation of the excitons and biexcitons. The signal now is given in terms of various Liouville pathways represented by the quasiparticle Green's functions.

In this work, instead of interpreting results of NEE simulation, we use the SOS method directly. As follows below from Eq. (13), the necessary ingredients to calculate SOS form of the signal include: (1) effective exciton/biexciton transition dipole moments; (2) their energies; (3) the corresponding dephasing rates. We propose to find (1) and (2) by comparing equation of motion for the independent (quasiparticles) and weakly interacting bosons. The lowest (1*S*) biexciton wavefunctions and energies are then found by the variational principle. Due to the shared valence band, exciton/biexciton coherence can be revealed as non-diagonal cross resonances in the 2D response, therefore allowing one to measure the biexciton binding or repulsion energies. Our model allows for possible lifting of degeneracy in the ortho-exciton manifold, which in turn alters the biexciton binding energy. The dephasing rates (3) are found from the phenomenological exciton/biexciton rate equations as discussed in Ref. [10]. The radiative, impurity induced and Auger processes destroy the coherence between the ground and exciton states; the rapid biexciton Auger destroys the biexciton and ground state coherence; the de-coherence between the exciton and biexciton is governed by two competing processes—biexciton Auger recombination and the loss rate of excitons given by their rate of binding (capturing) into biexcitons. Based on such a dephasing model we show that the ellipticity of the resonances is simply related to the initial biexciton/exciton density ratio.

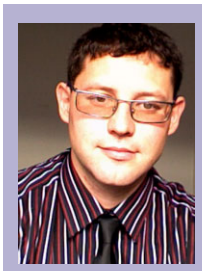

Oleksiy Roslyak received his Ph.D. in Theoretical Condensed Matter Physics from the City College of the City University of New York (CUNY) in 2007. His research interests include theoretical nanoscience of carbon based electronics; coherent 2D femtosecond spectroscopy; nonlinear spectroscopy with entangled photons and Quantum Optics. He currently works as a Research Associate at the Hunter College, CUNY.

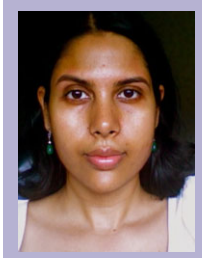

Upali Aparajita received her Ph.D. from the City University of New York in Theoretical Condensed Matter Physics. She has since worked as an Assistant Professor and a Postdoctoral Fellow in CUNY. Her research interests include superconductors, vortex dynamics, coherent 2D femtosecond spectroscopy and electronic transport in graphene nanostructures.

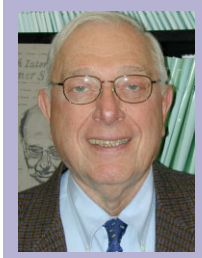

Joseph L. Birman is a Distinguished Professor of Physics at the City College of the City University of New York. He holds Ph.D. in Physics from Columbia University and Honorary Doctor of Science from University of Rennes, France. A prominent figure in the field of Theoretical Physics and author of "Theory of Infrared and Raman Scattering," Prof. Birman has been carrying out Theoretical Physics research with emphasis on condensed matter systems and the light emitting and electrical conductivity properties of solids for past 48 years.

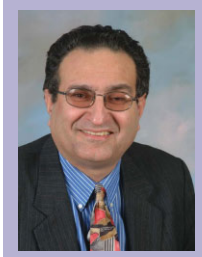

Shaul Mukamel is a Chancellor's Professor in Chemistry at University of California, Irvine. He holds a Ph.D. in Chemistry from the University of Tel Aviv, Israel. Professor Mukamel's interests focus on theoretical studies of ultrafast dynamics and relaxation processes of large molecules, biological complexes and semiconductors.

The quadrupole origin of the exciton, and in turn, exciton-biexciton transitions makes the corresponding oscillator strength dependent on the wave vector and polarization of the pulses. That is the quadrupole spectrum is chiral and the gaining or absorbing nature of the Liouville pathways depends on the sample orientation and polarization of the incoming and heterodyne pulses. Unlike in the molecular aggregates the chirality can be controlled by the crystal orientation. The orthogonal polarizations are treated as quantum bits (q-bits) thus making coherent 2D spectroscopy a possible tool for quantum computing. Such fs optical element opens new possibilities for future experiments. Specific crystal orientations and pulses polarization also provide the induced negative (gain) refractive index of the material. Cu_2O is a well-studied material but has not yet been experimentally explored with 2D femtosecond spectroscopy. Experiments to observe the biexcitons in Cu_2O should be straightforward, even at the one-quantum level, since they have been observed in GaAs quantum wells where the binding energy is significantly smaller than in Cu_2O [33]. Hence, we propose to utilize the corresponding exciton/biexciton coherence for lasing, which requires one to redirect the signal back to the crystal instead of measuring it by heterodyne detection.

2 Quadrupole biexciton formation and classification The yellow exciton in cuprous oxide (O_h) is formed by Coulomb interaction between electrons in the conduction band (Γ_6^+) and holes in the valence band (Γ_7^+),[1] within the direct band gap $E_{g,\mathbf{k}=0} = 2.17$ eV (See Fig. 1). The $1S$ excitons are given by the direct product of $e-h$ with the envelop function representation $\Gamma_1^+ \otimes \Gamma_6^+ \otimes \Gamma_7^+ = \Gamma_2^+ + {}^3\Gamma_5^+$. The triplet ${}^3\Gamma_5^+$ states are termed ortho-excitons (OE), while the singlet Γ_2^+ level is referred to as a para-exciton (PE). The levels are split by electron–hole exchange interaction, and the PE lie 12 meV below the OE [15]. This makes the $1S$ PE the lowest exciton level of cuprous oxide.

Due to the common even parity of the valence and conduction band the PE are optically forbidden. Note that this state may acquire some oscillator strength provided an external symmetry breaking to D_{2h} or D_{4h} by applying the stress on strong magnetic field. The OE are dipole-forbidden but quadrupole allowed ($\Gamma_{5,xy}^+, \Gamma_{5,yz}^+, \Gamma_{5,zx}^+$); triply degenerate.

Conventionally multi-excitons in cuprous oxide are described within a two-band model which neglects $\mathbf{k}$ dependent energy separation between different types of the OE, i.e., assumes degeneracy of the ${}^3\Gamma_5^+$ manifold, and possible OE/PE mixing by spin–orbit interaction [16]. The exciton pairs which are built from two yellow excitons can be classified by irreducible representation of their direct product:

$$\begin{aligned}\Gamma_6^+ \otimes \Gamma_7^+ \otimes \Gamma_6^+ \otimes \Gamma_7^+ &= \left(\Gamma_2^+ + \Gamma_5^+\right) \otimes \left(\Gamma_2^+ + \Gamma_5^+\right) \\ &= 2\Gamma_1^+ + \Gamma_3^+ + 3\Gamma_4^+ + \Gamma_5^+.\end{aligned} \tag{1}$$

[1] Note that all through the paper we use Koster notation of the representation, but when it is necessary indicate the degeneracy with the upper-script.

The biexciton Hamiltonian must be invariant under permutation of electrons (holes) of the two excitons. Hence, biexciton eigenstates must be characterized by two additional quantum numbers $\Gamma_{\alpha;\mu\nu}^+$; where $\alpha = \{1,3,4,5\}$; μ and ν denote the permutational parity ($\pm$).

The states $\Gamma_{\alpha;\pm,\pm}^+$ have an S-like envelope function, while $\Gamma_{\alpha;\pm\mp}^+$ have P-like envelope function. The two-exciton states are bound if their energy satisfies $E(\Gamma^+,\alpha;\mu\nu) < 2E(\Gamma_2^+)$. The only biexciton state satisfying this condition is the ground state $\Gamma_{1;--}^+$ [17]. It is worth to notice that ${}^3\Gamma_{4;-+}^+$ state may well satisfy the binding condition $E(\Gamma^+,4;-+) < 2E(\Gamma_4^+)$ and may form an ultra-short living biexciton. But in this work we focus our attention on the biexciton ground state. As shown in Appendix A, the Hamiltonian in terms of weakly interacting exciton creation(annihilation) operators $b_{\mathbf{k},i}^\dagger$ can be written as:

$$\begin{aligned}H = &\sum_{\mathbf{k}} \sum_{j=1}^{3} E_{\mathbf{k}}\left(\Gamma_{5,j}^+\right) b_{\mathbf{k},j}^\dagger b_{\mathbf{k},j} + \sum_{\mathbf{k}} E_{\mathbf{k}}\left(\Gamma_2^+\right) b_{\mathbf{k},4}^\dagger b_{\mathbf{k},4} \\ &+ \frac{1}{2V} \sum_{\mathbf{p},\mathbf{q},\mathbf{k}} \Bigg[\frac{1}{4}\left[U_{--} + 3U_{++}\right] \sum_{i=1}^{4} b_{\mathbf{p},i}^\dagger b_{\mathbf{q},i}^\dagger b_{\mathbf{q}+\mathbf{k},i} b_{\mathbf{p}-\mathbf{k},i} \\ &+ \sum_{i,j=1;i\neq j}^{4} U_{++} b_{\mathbf{p},i}^\dagger b_{\mathbf{q},j}^\dagger b_{\mathbf{q}+\mathbf{k},j} b_{\mathbf{p}-\mathbf{k},i} \\ &+ \frac{1}{4} \sum_{i,j=2;i\neq j}^{4} (-1)^{i+j} [U_{--} - U_{++}] b_{\mathbf{p},i}^\dagger b_{\mathbf{q},i}^\dagger b_{\mathbf{q}+\mathbf{k},j} b_{\mathbf{p}-\mathbf{k},j} \\ &+ \frac{1}{4} \sum_{i=2}^{4} (-1)^{i+1} [U_{++} - U_{--}] \\ &\times \left(b_{\mathbf{p},i}^\dagger b_{\mathbf{q},i}^\dagger b_{\mathbf{q}+\mathbf{k},1} b_{\mathbf{p}-\mathbf{k},1} + b_{\mathbf{p},1}^\dagger b_{\mathbf{q},1}^\dagger b_{\mathbf{q}+\mathbf{k},i} b_{\mathbf{p}-\mathbf{k},i} \right) \Bigg].\end{aligned} \tag{2}$$

Here V stands for the volume of the sample, and $U_{\pm\pm}(\mathbf{p},\mathbf{q},\mathbf{p}-\mathbf{k},\mathbf{q}+\mathbf{k})$ are the Fourier transforms of the exciton Coulomb scattering matrix elements. These are calculated with the two-exciton wave functions that are either symmetric or asymmetric under permutations of the spin projections of the two electrons as well as under permutations of the total angular-momentum projections of the two holes. For small exciton momenta one can use the random phase approximation [16]. This gives energy $U_{++}(0) = -U_{--}(0) \propto Ry_{1S} a_X^3$, where $Ry_{1S} = 153$ meV is the ionization potential of the quadrupole exciton.

Note that in the above we did not use the PE/OE basis (two level model) which is conventionally used for exciton description in cuprous oxide. First the OE/PE separation is not rigorous but conditional. Indeed, in this material the hole states involve a non-zero orbital momentum (the actual hole bands are made up of 3d Cu^+ orbitals) and cannot be characterized by a total spin and its projection of two particles. Second reason is that we do not know *a priori* the relation between biexciton binding energy $E_{XX;\Gamma_1^+}$ (for

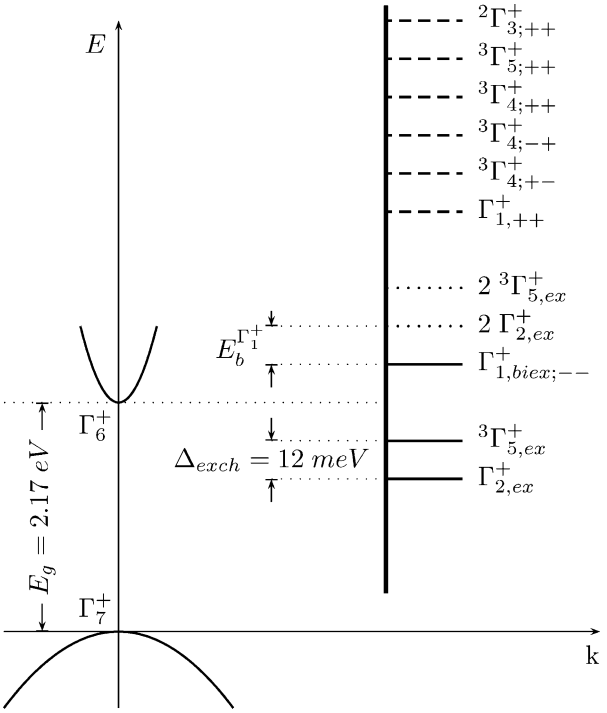

Figure 1 The cuprous oxide band structure at $\mathbf{k} = 0$ (Γ point) and the corresponding exciton, two-exciton and biexciton states. The one and two-exciton manifolds consist of the singlet Γ_2^+ (PE) and triplet $^3\Gamma_5^+$ (OE). The lowest optically forbidden states of the biexcitons are formed by the Coulomb interaction and denoted as asymmetric $\Gamma^+_{1,--}$ and symmetric $\Gamma^+_{1,---}$. This can be revealed through their coherence with the two-exciton states. The rest of the bounded and non-bounded states are shown but not investigated in the present paper.

brevity we hereafter omit the subscript Γ_1^+) and exchange splitting Δ_{exch} between the OE and PE. Whereas the PE/OE approach implies that this two types are well separated. Nevertheless, it was demonstrated by Bobrysheva and Moskalenko [18] that the cuprous oxide biexcitons are stable even for large ortho–para splitting $E_{\text{XX};\Gamma_1^+} \ll \Delta_{\text{exch}}$. However, in this case the biexciton binding energy is twice smaller than it is in case of small splitting $E_{\text{XX};\Gamma_1^+} \gg \Delta_{\text{exch}}$. We addressed this effect by two times reducing the effective exciton–exciton interaction (see Section 4 for more details).

As the result, the above Hamiltonian contains attractive interaction between $\Gamma^+_{5,xz}$ and $\Gamma^+_{5,yz}$ only, while the PE/OE approximation does not distinguish between different OE [16]. The second term in the Hamiltonian (2) indicates that excitons of the same species cannot form a bound state, and the third term implies that the overall exciton interaction is repulsive. The detailed description of each contributing term can be found in Appendix A.

The exciton interaction with the optical field has the form:

$$H_{\text{int}} = \sum_{j=1}^{4} \sum_{\mathbf{k},i=1}^{3} \delta_{\mathbf{k},\mathbf{k}_j} \mathbf{E}_j(\mathbf{k},t) \mathbf{d}_i(\mathbf{k}, \mathbf{E}/E) \left[b^\dagger_{\mathbf{k},i} + b_{\mathbf{k},i} \right],$$

where $\mathbf{k}_i = \{\mathbf{k}_1, \mathbf{k}_2, \mathbf{k}_3, \mathbf{k}_{\text{III}}\}$ and $\mathbf{E}(\mathbf{k}, t)$ is the electric field of the photons (see Fig. 2 for details).

The effective dipole moments due to the quadrupole transitions are related to the experimentally measurable oscillator strength f as:

$$\begin{aligned} \mathbf{d}_1 &= \mathbf{d}_{yz} \propto \sqrt{f}(\mathbf{e}_2 k_z + \mathbf{e}_3 k_y) \\ \mathbf{d}_2 &= \mathbf{d}_{xz} \propto \sqrt{f}(\mathbf{e}_1 k_z + \mathbf{e}_3 k_x) \\ \mathbf{d}_3 &= \mathbf{d}_{xy} \propto \sqrt{f}(\mathbf{e}_1 k_y + \mathbf{e}_2 k_x). \end{aligned} \tag{3}$$

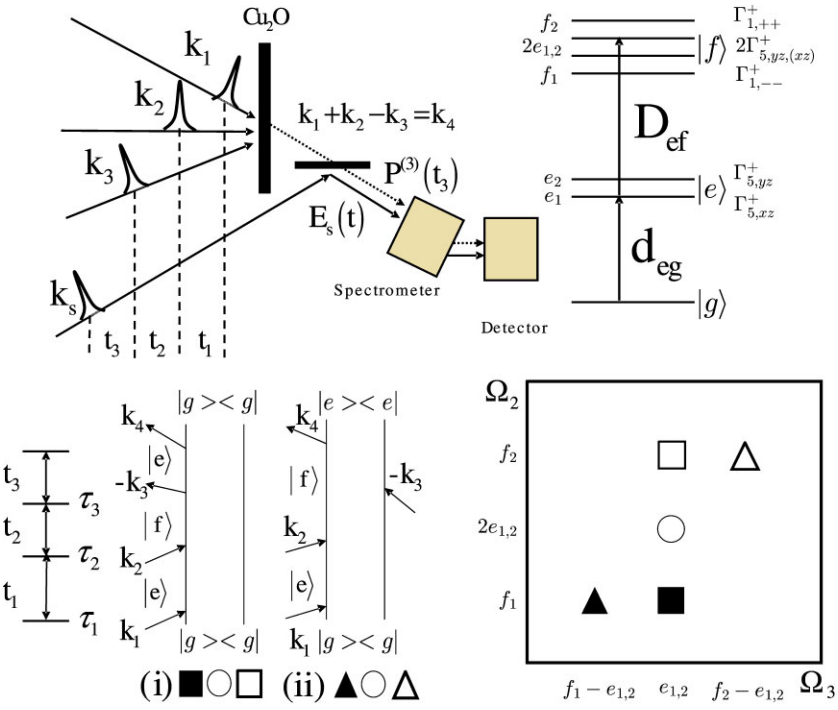

Figure 2 (online colour at: www.pss-b.com) The proposed experimental set up for the 2D quadrupole spectroscopy of the cuprous oxide oriented sample. The symbols $\mathbf{d}_{\text{eg}}$ and $\mathbf{D}_{\text{ef}}$ represent the dipole moments of the quadrupole allowed transitions from the ground state $|g\rangle$ to the one-exciton $|e\rangle = \Gamma^+_{5,yz}, \Gamma^+_{5,xz}$ and two-exciton $|f\rangle = \Gamma^+_{1,--}, 2\Gamma^+_{5,yz}, 2\Gamma^+_{5,xz}, \Gamma^+_{1,++}$ states correspondingly. The $\mathbf{k}_{\text{III}}$ related Feynman diagrams illustrate the absorptive (i) and gain (ii) contributions to the $S^{(3)}$ response function.

The quadrupole nature of the OE makes the non-linear response chiral, i.e., it depends on the corresponding wave vector and polarization of the optical pulses and heterodyne through the effective dipole moments (3). It is analogous to the chiral response of organic molecular aggregates [19] but unlike them the quadruple chirality can be controlled by the crystal orientation. In the next section we investigate the causal non-linear $\chi^{(3)}$ response of the cuprous oxide crystal and some chirality effects on the spectra.

3 Correlation spectroscopy of quadrupole biexcitons In analogy with nuclear magnetic resonance [20], 2D-spectroscopy has recently been implemented to study electronic and vibrational coupling in molecules [21–23] and in semiconductors [24–26]. In this section we utilize the unique sensitivity of this spectroscopy to couplings among various exciton resonances to predict the spectral signatures of biexcitons in cuprous oxide. We use the excited state absorption part of the general four wave mixing signal heterodyne detected in the following phase matching direction $\mathbf{k}_{\mathrm{III}} = \mathbf{k}_1 + \mathbf{k}_2 - \mathbf{k}_3$. The first two pulses promote the coherence between the ground state and exciton (during t_1 interval) then two-exciton (t_2 interval) states. The third pulse probes the formation of the biexciton during t_3 interval. Depending on whether it interacts with the ket or with the bra, one has two possible Liouville pathways. In one of these pathways the third pulse dexcites the two-exciton ket and makes the coherence between the exciton and the ground state. In the other pathway the third pulse excites the bra and creates the coherence between the exciton and two-exciton manifolds. The signal arises from the third order polarization:

$$P_{\sigma}^{(3)}(t) = \sum_{\alpha,\beta,\gamma} \int_0^{\infty}\int_0^{\infty}\int_0^{\infty} \mathrm{d}t_1\mathrm{d}t_2\mathrm{d}t_3 S^{(3)}_{\sigma,\alpha,\beta,\gamma}(t_1,t_2,t_3) \times E_{\gamma}(t-t_3)E_{\beta}(t-t_3-t_2)E_{\alpha}(t-t_3-t_2-t_1) \tag{4}$$

and can be heterodyne detected with the fourth pulse at time t. To study the biexciton formation it is convenient to define 2D spectrum by the Fourier transform of the response function with respect to t_2 and t_3, keeping time interval t_1 as a control parameter (see Fig. 2):

$$S^{(3)}_{\sigma,\alpha,\beta,\gamma}(t_1,\Omega_2,\Omega_3) = \int_0^{\infty}\int_0^{\infty} \mathrm{d}t_2\mathrm{d}t_3 S^{(3)}_{\sigma,\alpha,\beta,\gamma}(t_1,t_2,t_3)\mathrm{e}^{i\Omega_2 t_2 + i\Omega_3 t_3}. \tag{5}$$

To calculate this response function we take into account the only optically active excitonic transitions $\left|\Gamma^{+}_{5;yz}\right\rangle = b^{\dagger}_{\mathbf{k},1}|g\rangle$ and $\left|\Gamma^{+}_{5;xz}\right\rangle = b^{\dagger}_{\mathbf{k},2}|g\rangle$ which are capable of forming the lowest biexciton states due to their mutual attraction. Using the center of mass approach one can introduce the symmetric (++) and asymmetric (−−) biexciton creation operators for the lowest biexciton states:

$$\begin{aligned}\left|\Gamma^{+}_{1,\pm\pm}\right\rangle &= B^{\dagger}_{\mathbf{K},\pm\pm,1S}|g\rangle \\ &= \frac{1}{2\sqrt{V}}\sum_{\mathbf{l}} \Psi_{1S,\mathbf{l}}\left(b^{\dagger}_{\mathbf{l}+\mathbf{K}/2,1}b^{\dagger}_{-\mathbf{l}+\mathbf{K}/2,1} \mp b^{\dagger}_{\mathbf{l}+\mathbf{K}/2,2}b^{\dagger}_{-\mathbf{l}+\mathbf{K}/2,2}\right)|g\rangle,\end{aligned} \tag{6}$$

where $\mathbf{K}$ and $\mathbf{l}$ are the wave vectors of the center of mass and relative motion of the excitons constituting the biexciton; $\Psi_{J,\mathbf{l}}$ is the biexciton envelope function (for the lowest biexciton state the angular momentum of the exciton molecule J is equal to $1S$).

The commutation relations for the exciton and biexciton operators are given by:

$$\begin{aligned}\left[b_{\mathbf{l},i}, b^{\dagger}_{\mathbf{l}',j}\right] &= \delta_{\mathbf{l},\mathbf{l}'}\delta_{i,j} + O\left(n_{\mathrm{e}}a_{\mathrm{X}}^3\right), \\ \left[B_{\mathbf{K},i}, B^{\dagger}_{\mathbf{K}',j}\right] &= \delta_{\mathbf{K},\mathbf{K}'}\delta_{i,j} + O\left(n_{\mathrm{f}}a_{\mathrm{XX}}^3\right), \\ \left[B_{\mathbf{K},\Gamma^{+}_{1,++}}, b^{\dagger}_{\mathbf{k},1(2)}\right] &= \pm\frac{1}{2\sqrt{V}} \times \left(\Psi^{*}_{\Gamma^{+}_{1},\mathbf{K}/2-\mathbf{k}} + \Psi^{*}_{\Gamma^{+}_{1},\mathbf{k}-\mathbf{K}/2}\right)b_{\mathbf{K}-\mathbf{k},1(2)}, \\ \left[B_{\mathbf{K},\Gamma^{+}_{1,--}}, b^{\dagger}_{\mathbf{k},1(2)}\right] &= \frac{1}{2\sqrt{V}} \times \left(\Psi^{*}_{\Gamma^{+}_{1},\mathbf{K}/2-\mathbf{k}} + \Psi^{*}_{\Gamma^{+}_{1},\mathbf{k}-\mathbf{K}/2}\right)b_{\mathbf{K}-\mathbf{k},1(2)}.\end{aligned} \tag{7}$$

Here $n_{\mathrm{e(f)}}$ and $a_{\mathrm{X(XX)}}$ are the exciton (biexciton) density and Bohr radius correspondingly. $O(n_{\mathrm{e}}a_{\mathrm{X}}^3)$ and $O(n_{\mathrm{f}}a_{\mathrm{XX}}^3)$ are the contributions from the phase-filling factor and show the deviation of the excitons and biexcitons from the true bosons. At low exciton density ($n_{\mathrm{e}}a_{\mathrm{X}}^3 \ll 1$) the equation of motion for the exciton and biexciton states in the center of mass approximation assume the form (29,30) and (31,32), see Appendix B. The increase of the electron/hole density leads at first to the disappearance of the biexcitons as bound compound quasiparticles. With further increase in the excitation level, the excitons begin to dissociate too, and our model is no longer applicable.

The second terms in the equation of motion for the biexciton (31,32) are due to broken ortho (para) - symmetry of the excitons. Due to an external perturbation, the degeneracy of the ${}^{3}\Gamma^{+}_{5;\mathbf{k}}$ excitonic levels can be lifted. Therefore, the biexciton can be formed by hybridization of the two-exciton transitions (see Section 4 for details).

Let us first consider the conventional biexciton formation and neglect possible lifting of the OE degeneracy. To proceed further and obtain the non-linear signal in SOS form we also need equations of motion in terms of an effective independent-Boson model for exciton and biexciton quasiparticles. To do so, we recall that in case of exciton condensation the average value of the creation (destruction) operator is a macroscopically large quantity $\langle b_{\mathbf{k}}\rangle/\sqrt{V} = \langle b_0\rangle/\sqrt{V} = -\sqrt{n_0}$, where the condensate density $n_0 \le n_{\mathrm{e}}$.

We also take into account the small Bohr radius of the quadrupole biexciton within the hydrogen-like envelope function approximation:

$$\Psi_{\Gamma_1^+,\mathbf{l}} = \frac{8\sqrt{\pi a_{\mathrm{XX}}^3}}{\left(1 + l^2 a_{\mathrm{XX}}^2\right)^2}. \tag{8}$$

This gives the following estimate for the average value of the last two commutators in Eq. (7):

$$\begin{aligned}
&\pm\frac{1}{2\sqrt{V}}\left(\Psi^*_{\Gamma_1^+,\mathbf{K}/2-\mathbf{k}} + \Psi^*_{\Gamma_1^+,\mathbf{k}-\mathbf{K}/2}\right)\left\langle b_{\mathbf{K}-\mathbf{k},1(2)}\right\rangle \\
&= \pm\frac{1}{2\sqrt{V}}\left(\Psi^*_{\Gamma_1^+,-\mathbf{K}/2} + \Psi^*_{\Gamma_1^+,\mathbf{K}/2}\right)\left\langle b_{0,1(2)}\right\rangle \\
&= O\left(\sqrt{n_0 a_{\mathrm{X}}^3}\right).
\end{aligned}$$

The commutators (7) can be therefore simplified in the limit of small biexciton and exciton density $n_{\mathrm{e}}a_{\mathrm{X}}^3 \ll \sqrt{n_{\mathrm{e}}a_{\mathrm{X}}^3} \ll n_{\mathrm{f}}a_{\mathrm{XX}}^3 \ll 1$ to:

$$\begin{aligned}
&\left[b_{\mathbf{l},i}, b^\dagger_{\mathbf{l}',j}\right] = \delta_{\mathbf{l},\mathbf{l}'}\delta_{i,j}; \qquad \left[B_{\mathbf{K},i}, B^\dagger_{\mathbf{K}',j}\right] = \delta_{\mathbf{K},\mathbf{K}'}\delta_{i,j}; \\
&\left[B_{\mathbf{K},\Gamma^+_{1,++}}, b^\dagger_{\mathbf{k},1(2)}\right] = 0; \quad \left[B_{\mathbf{K},\Gamma^+_{1,--}}, b^\dagger_{\mathbf{k},1(2)}\right] = 0.
\end{aligned} \tag{9}$$

In this case the bosonic Hamiltonian (the interaction between excitons is given implicitly in the energy of the two-exciton manifold) has the form:

$$\begin{aligned}
H = &\sum_{\mathbf{k}} E\left(\Gamma^+_{5,yz,\mathbf{k}}\right) b^\dagger_{\mathbf{k},1} b_{\mathbf{k},1} + E\left(\Gamma^+_{5,xz,\mathbf{k}}\right) b^\dagger_{\mathbf{k},2} b_{\mathbf{k},2} \\
&+ \sum_{\mathbf{K}} E\left(\Gamma^+_{1,++,\mathbf{K}}\right) B^\dagger_{\mathbf{K},\Gamma^+_{1,++}} B_{\mathbf{K},\Gamma^+_{1,++}} \\
&+ E\left(\Gamma^+_{1,--,\mathbf{K}}\right) B^\dagger_{\mathbf{K},\Gamma^+_{1,--}} B_{\mathbf{K},\Gamma^+_{1,--}} \\
&- \sum_{\mathbf{K},j}^{4} \mathbf{E}\cdot\mathbf{D}_1^{++}(\mathbf{K},\mathbf{k}_j)\left(B^\dagger_{\mathbf{K},\Gamma^+_{1,++}} b_{\mathbf{k}_j,1} + b^\dagger_{\mathbf{k}_j,1} B_{\mathbf{K},\Gamma^+_{1,++}}\right) \\
&- \sum_{\mathbf{K},j}^{4} \mathbf{E}\cdot\mathbf{D}_2^{++}(\mathbf{K},\mathbf{k}_j)\left(B^\dagger_{\mathbf{K},\Gamma^+_{1,++}} b_{\mathbf{k}_j,2} + b^\dagger_{\mathbf{k}_j,2} B_{\mathbf{K},\Gamma^+_{1,++}}\right) \\
&- \sum_{\mathbf{K},j}^{4} \mathbf{E}\cdot\mathbf{D}_1^{--}(\mathbf{K},\mathbf{k}_j)\left(B^\dagger_{\mathbf{K},\Gamma^+_{1,--}} b_{\mathbf{k}_j,1} + b^\dagger_{\mathbf{k}_j,1} B_{\mathbf{K},\Gamma^+_{1,--}}\right) \\
&- \sum_{\mathbf{K},j}^{4} \mathbf{E}\cdot\mathbf{D}_2^{--}(\mathbf{K},\mathbf{k}_j)\left(B^\dagger_{\mathbf{K},\Gamma^+_{1,--}} b_{\mathbf{k}_j,2} + b^\dagger_{\mathbf{k}_j,2} B_{\mathbf{K},\Gamma^+_{1,--}}\right) \\
&- H_{\mathrm{int}}.
\end{aligned} \tag{10}$$

Here we have introduced the exciton/biexciton dipole transition moment $\mathbf{D}(\mathbf{K},\mathbf{k}_i)$ and the biexciton manifold energy $E(\Gamma^+_{1,++,\mathbf{K}})$, $E(\Gamma^+_{1,--,\mathbf{K}})$. The corresponding equations of motion obtained by using the independent boson model are given in Appendix B, Eqs. (33–36). Note that Eqs. (33,34) are different from Eqs. (30,31) due to simplified commutation rules [27].

Comparing Eqs. (31,32) with (35,36) we obtain the biexciton energy:

$$\begin{aligned}
E\left(\Gamma^+_{1,\pm\pm},\mathbf{K}\right) = &E\left(\Gamma^\dagger_{5,yz},\mathbf{K}/2\right) + E\left(\Gamma^\dagger_{5,xz},\mathbf{K}/2\right) \\
&\mp\frac{1}{4V^2}\sum_{\mathbf{l},\mathbf{l}'}[U_{--} - U_{++}]\Psi^*_{\Gamma_1^+,\mathbf{l}'}\Psi_{\Gamma_1^+,\mathbf{l}}.
\end{aligned} \tag{11}$$

The corresponding transition dipole moments of exciton/biexciton:

$$\begin{aligned}
\mathbf{D}_1^{++}(\mathbf{K},\mathbf{k}_j) &= \frac{\mathbf{d}_1(\mathbf{k}_j)}{\sqrt{V}}\left(\Psi_{\Gamma_1^+,\mathbf{K}/2-\mathbf{k}_j} + \Psi_{\Gamma_1^+,\mathbf{k}_j-\mathbf{K}/2}\right) \\
\mathbf{D}_2^{++}(\mathbf{K},\mathbf{k}_j) &= -\frac{\mathbf{d}_2(\mathbf{k}_j)}{\sqrt{V}}\left(\Psi_{\Gamma_1^+,\mathbf{K}/2-\mathbf{k}_j} + \Psi_{\Gamma_1^+,\mathbf{k}_j-\mathbf{K}/2}\right) \\
\mathbf{D}_1^{--}(\mathbf{K},\mathbf{k}_j) &= \frac{\mathbf{d}_1(\mathbf{k}_j)}{\sqrt{V}}\left(\Psi_{\Gamma_1^+,\mathbf{K}/2-\mathbf{k}_j} + \Psi_{\Gamma_1^+,\mathbf{k}_j-\mathbf{K}/2}\right) \\
\mathbf{D}_2^{--}(\mathbf{K},\mathbf{k}_j) &= \frac{\mathbf{d}_2(\mathbf{k}_j)}{\sqrt{V}}\left(\Psi_{\Gamma_1^+,\mathbf{K}/2-\mathbf{k}_j} + \Psi_{\Gamma_1^+,\mathbf{k}_j-\mathbf{K}/2}\right).
\end{aligned} \tag{12}$$

The biexciton energy in Eq. (11) can be minimized using an appropriate trial wave function, thereby one can obtain the effective dipole moments (12). Thus one can calculate the Green's functions of the bosonic equations of motion for exciton/biexciton and, as it was discussed in the Introduction, the response function (5) can be recast in a SOS form [21]:

$$\begin{aligned}
&S^{(3)}_{\sigma,\alpha,\beta,\gamma}(t_1,\Omega_2,\Omega_3) \\
&= \frac{d^\sigma_{\mathrm{eg}} D^\gamma_{\mathrm{e'f}} D^\beta_{\mathrm{ef}} d^\alpha_{\mathrm{ge}} \exp(-iE_{\mathrm{eg}}t_1 - \hbar\gamma_{\mathrm{eg}}t_1)}{(E_{\mathrm{fg}} - \hbar\Omega_2 + i\hbar\gamma_{\mathrm{fg}})(E_{\mathrm{e'g}} - \hbar\Omega_3 + i\hbar\gamma_{\mathrm{e'g}})} \\
&- \frac{D^\sigma_{\mathrm{fe'}} d^\gamma_{\mathrm{ge'}} D^\beta_{\mathrm{ef}} d^\alpha_{\mathrm{ge}} \exp(-iE_{\mathrm{eg}}t_1 - \hbar\gamma_{\mathrm{eg}}t_1)}{(E_{\mathrm{fg}} - \hbar\Omega_2 + i\hbar\gamma_{\mathrm{fg}})(E_{\mathrm{fe'}} - \hbar\Omega_3 + i\hbar\gamma_{\mathrm{fe'}})}.
\end{aligned} \tag{13}$$

Here the subscript g is the ground state; e, e′ stand for the exciton manifold $\Gamma^+_{5,yz}$, $\Gamma^+_{5,xz}$, $\Gamma^+_{5,xy}$ and f runs over the biexciton manifold ($\Gamma^+_{1,++}$, $\Gamma^+_{1,--}$); the super-script at the exciton $\mathbf{d}_{\mathrm{eg}}$ and two-exciton $\mathbf{D}_{\mathrm{ef}}$ transition dipoles denotes the projection on the electric field of the corresponding pulses.

The imaginary part of the response function (13) gives the non-linear absorption of the previous pulse by the system whose refractive index is modified by the other pulses. Therefore the absorption can be either positive or negative depending on the pulse polarization and timing, while the real part of the response function reveals the dispersive properties of the induced refraction. Consequently, for dipole-allowed transitions, the first term in the response function (13) is referred to as the absorptive terms (See the Feynman diagram (i) in Fig. 2). The second set of terms is referred as gain terms (diagram (ii)). For the chiral quadrupole transition the gain or absorptive nature of each term in the response function may be controlled by the crystal

orientation and laser polarizations. The difference between these two contributions is determined during the t_3 interval when the two excitons are interacting. The mutual exciton scattering is the source of the non-linear signal. If it were not so, this two terms would cancel each other. In other words, there are no cross resonances along $\hbar\Omega_3 = 2e_{1,2}$ in the corresponding 2D spectrum (see more details in Section 4).

We recall that instead of resorting to the bosonic form of the equation of motion one can obtain the Green's functions for the weakly interacting exciton model given by the Hamiltonian (2) using NEE approach. In this case the complete set (not only the lowest states investigated here) of biexcitons are given by the poles of the scattering matrix. In the recent work of *S*. Mukamel et.al. [28] the authors demonstrated intimate connection between the SOS and NEE approaches, the pros and cons of the model. Although the NEE provide more detailed than SOS description of the phenomena, it requires computing the scattering matrix which would require numerical solution of the Bethe-Selpeter many body equation, which is an expensive computational task. Hence, this paper is focused on demonstrating how one can be able to observe the dark biexciton formation by utilizing methods of non-linear femtosecond spectroscopy. Our SOS model is rather simple and therefore can describe only the lowest biexcitons but cannot determine the biexciton dependence on the exciton density or screening. It is rather a guideline for future experiments than a complete ab initio simulation. We anticipate that such experiments would be able to prove (or disprove) the biexciton existence in cuprous oxide. In the next section we investigate the 2D quadrupole spectrum under different excitation conditions and sample orientations.

4 Numerical results and discussion Unfortunately there is no simple analytic solution of Eq. (11) and one must resort to an approximate solution for simulation of the 2D spectrum (13). Here we use 1*S* trial wave function (8) to minimize the biexciton energy (11) with respect to the variational parameter (biexciton radius) a_{XX}. We assume the following form of the exciton–exciton interaction up to the third order in the exciton radius [29]:

$$U_{\pm\pm} = \pm\frac{26\pi}{3} Ry_{1S} a_X^3 \left[1 + \frac{1}{(1 + a_X^3 m_e^2 |\mathbf{l} - \mathbf{l}'|^2 / m_X^2)}\right]^{-1}. \tag{14}$$

As we mentioned earlier, the factor $26\pi/3$ is half of the regular $52\pi/3$ on account of large ortho-para splitting. The exciton effective mass $m_e^2/m_X^2 = 0.14$, binding energy $Ry_{1S} = 153$ meV and Bohr radius $a_X = 5.1\,\mathring{A}$ are given by the "central cell correction" model [1]. They are modified by non-parabolicity of the conduction and valence bands, the coupling of the exciton electron and hole with the longitudinal optical phonons and by the dielectric function dependence on the distance between the electron and hole. The original parameters (without central cell correction) the reader can find, for instance, in Ref. [16]. The corrections are essential in cuprous oxide and affect not only the exciton but also biexciton parameters. This is one of the reasons why we make our own numerical estimates of the biexciton binding energy rather than simply citing already existing results.

The expression above is valid for $|\mathbf{l} - \mathbf{l}'| < m_X/m_h a_X = 3.9/a_X$. Therefore the summation can be changed into integration:

$$\frac{1}{V}\sum_{\mathbf{l}} \to \frac{1}{\pi^2}\int_0^{3.9/a_X} l^2 d\mathbf{l}.$$

Numerical simulation yields that the minimum of the biexciton energy (11) occurs at $a_{XX} = 165\,\mathring{A}$. This corresponds to the biexciton binding energy $E_{XX} = 0.031 Ry_{1S} = 4.743$ meV. The corresponding biexciton oscillator strength is therefore given by [16]: $f_{XX}/f_X = (a_{XX}/a_X)^3 = 3.4 \times 10^4$. Now let us comment on the accuracy of our approach compared to those previously reported in the literature. A variational calculation by [31] yields a biexciton binding energy 3.3 meV. More elaborate variational calculations by [18] gives 6.2 meV. In contrast, Huang [32] applied a Feynman's path-integral approach to the general biexciton binding energy and predicted 13 meV for our electron–hole mass ratio. Since there were no direct observation of the biexciton formation, our simple model is just as good as others, and serve here more illustrative point. As well as some approximation for the transition moments.

Since biexciton formation is always accompanied by Auger recombination, we assume that the ground state of the system has finite densities of thermalized exciton n_e and biexcitons n_f at the temperature of 70 (40) K. Note that this does not affect our statement that first two pulses promote the system from its ground state, since out of all possible multi-exciton formation we consider only the biexcitons. The laser pulses promote the excitons or biexcitons from the thermal ground state distribution and the subsequent system relaxation is described by the kinetic equations [7]:

$$\begin{aligned} \frac{dn_e}{dt} &= -\frac{n_e}{\tau} + \frac{n_f}{\tau_A} - 2\overline{C} n_e^2 + 2\overline{C} n^* n_f \\ \frac{dn_f}{dt} &= -\frac{n_f}{\tau_A} + \overline{C} n_e^2 - \overline{C} n^* n_f. \end{aligned} \tag{15}$$

Here $2\overline{C} = 10^{-16}$ cm^3/ns is the average recombination (capture) coefficient; $\tau_A = 70$ ns is the biexciton lifetime [3]; τ is the exciton life time which is mostly defined by impurities and assumed to be much lager then the Auger life time τ_A. Note that $\overline{C}$ is much lager than the conventional exciton (biexciton) Auger rate. The reason is that the conventional Auger process involves the recombination in this forbidden direct-gap crystal.

The mass-action equilibrium density is given by:

$$n^*(T) = \frac{n_e^2}{n_f} = \left(\frac{mk_BT}{4\pi\hbar^2}\right)^{3/2} e^{-E_{XX}/k_BT},$$

where the biexciton mass is assumed to be twice the free exciton mass m. The response function (13) dynamics (t_2, t_3) occurs on the fs time scale, whereas the population dynamics is much slower (ps to ns). Therefore we treat the lifetime as the dominant dephasing mechanism. From Eq. (15) it is straightforward to deduce the effective dephasing rates for the ground state to the exciton (biexciton) transitions:

$$\begin{aligned}\gamma_{eg} &= \frac{1}{\tau} + 2\overline{C}n \\ \gamma_{fg} &= \frac{1}{\tau_A} + \overline{C}n^*.\end{aligned} \tag{16}$$

As for the exciton/biexciton dephasing rate we notice that the loss of the excitons contribute to the gain of the biexcitons as $\overline{C}n_e^2$ and the loss of the biexcitons contributes to the gain of the exciton manifold as $n_f/\tau_A + 2\overline{C}n^*n_f$. Both processes contribute to the exciton/biexciton dephasing:

$$2\gamma_{ef} = \frac{1}{\tau_A} + 2\overline{C}n^* + \overline{C}n_e. \tag{17}$$

In Fig. 3, we present the 2D correlation spectrum when the system is initially at equilibrium $n_e = n_f = n^* = 1.2 \times 10^{18}\ \mathrm{cm}^{-3}$, and the non-equilibrium exciton/biexciton distribution $n_f \ll n_e$. The cross-resonances in Fig. 3 indicate the correlation between the exciton ($\Gamma^+_{5,yz}$, $\Gamma^+_{5,xz}$) and two-exciton ($\Gamma^+_{1,--}$, $2\Gamma^+_{5,yz}$, $2\Gamma^+_{5,xz}$, $\Gamma^+_{1,++}$) manifolds schematically presented in Fig. 2. Note that the central cross resonance (correlation between one exciton e and two non-interacting excitons $2e$) is not visible due to much smaller two-exciton transition oscillator strength comparing to those of biexcitons. For the given crystal orientation and laser polarizations the Feynman diagram (i) is absorptive and diagram (ii) shows gain (see also Fig. 2). At higher temperature ($T = 70\,\mathrm{K}$) the cross resonances are slightly shifted due to non-resonant contributions. And the cross resonances are elongated along the $\hbar\Omega_3$ axis due to higher biexcitons dephasing rate. The elongation is not due to disorder as has been observed in other experiment [33]. For the non-equilibrium case ($n_f < n_e$) this effect is less pronounced.

We next examine the chiral properties of the quadrupole 2D spectrum. Since both exciton and biexciton transition dipole moments depend on the wave vector we vary the crystal orientation and laser polarization $T = 40\,\mathrm{K}$ (see Figs. 4 and 5). An interesting practical application of chirality is to an optical logical element for quantum computing. If one defines the signal polarization as a qubit $\mathbf{E}^{\perp} = 1$, $\mathbf{E}^{\parallel} = 0$ then the logical OR between the second and the third pulses can be probed by the fourth signal for the $\mathbf{k} = [112]$ crystal orientation. Indeed, $\mathbf{E}_4^{\parallel}$ reveals this logical operation at the exciton-biexciton resonance $\hbar\Omega_2 = 4.0597\,\mathrm{eV}$ and $\Omega_3 = 2.0322\,\mathrm{eV}$. A more thorough investigation of the quantum computing possibilities by utilizing the quadrupole chirality and coherency between excitons and biexcitons will be of interest.

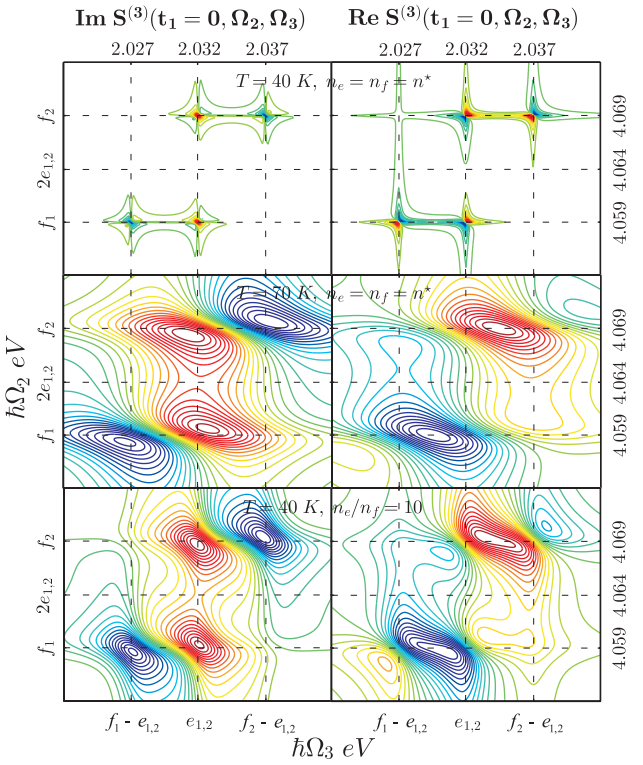

Figure 3 (online colour at: www.pss-b.com) 2D correlation spectrum of the cuprous oxide. The Im part correspond to the non-linear absorption and Re part reveals the dispersion. The laser pulses are oriented parallel to the $\mathbf{E}_j||[001]$ direction and $\mathbf{k}_j||[110]$.

Another fascinating effect of quadrupole chirality along the main axis of the crystal ($\mathbf{k}||[001]$ or $\mathbf{k}||[110]$) is revealed by the coherent signals. For these crystal orientations it is possible to select either absorptive or gain terms of the response function (See Fig. 5). The possibility of gain only allows one to have lasing at the corresponding $\Omega_2 + \Omega_3$ frequency, the absorptive terms will allow laser field detection at those frequencies.

To achieve the lasing, instead of heterodyne detecting $\mathbf{k}_{III}$ signal, we split it in two beams and direct it back into the crystal in the following fashion. The first beam serves as $\mathbf{k}_2$ signal and the second is $\mathbf{k}_3$. The laser energy is provided by the one-exciton manifold ($\mathbf{E}_1^2$) and the necessary coherence is given by the coherence between the one-exciton and two-exciton manifold ($-\mathbf{k}_3$). Lasing occurs at the frequency specified by the given time delays between pulses. Although the efficiency of the proposed lasing per cycle $\mathbf{E}_4^2/\mathbf{E}_1^2$ is low due to the small oscillator strength of the quadrupole transitions and rather small radius of the biexciton, the proposed laser will have very narrow line-width determined by the exciton/biexciton dephasing rate (17).

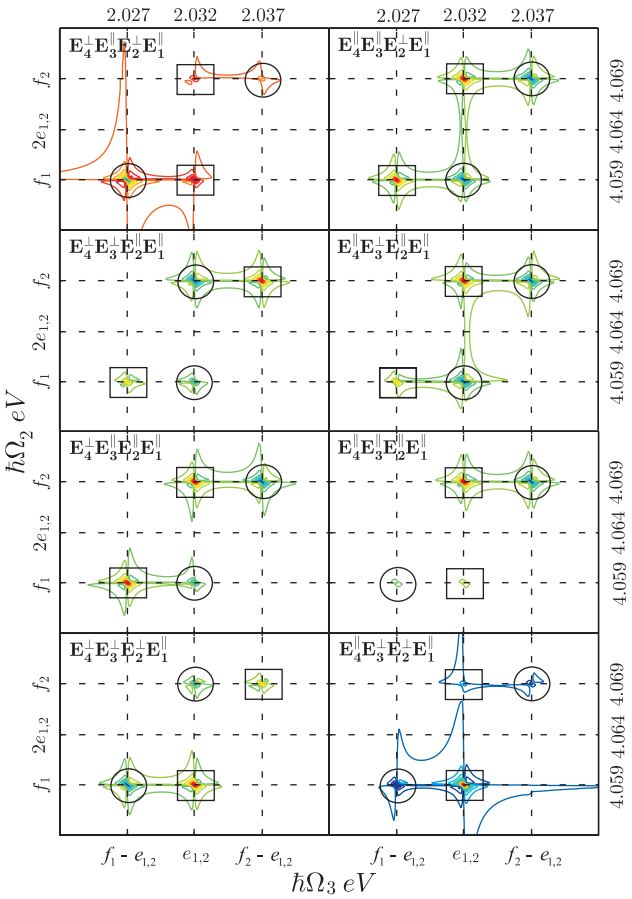

Figure 4 (online colour at: www.pss-b.com) Chirality effects in the 2D quadrupole correlation spectrum $\Im S^{(3)}(t_1 = 0, \Omega_2, \Omega_3)$ for the cuprous oxide, $T = 40$ K, $n_e = n_f$. The sample is oriented in $\mathbf{k}_j \| [112]$ direction and we used the notation $\mathbf{E}_j^{\parallel} \| [11\bar{1}]$, $\mathbf{E}_j^{\perp} \| [1\bar{1}0]$. The squares mark the absorptive and circles stand for gaining contributions to the response function.

So far we have considered the case of the degenerate OE level Γ_5^+. Now let us turn to a general case when the degeneracy may be lifted. In this case the biexciton branches are further split. To describe this effect we note that the equations of motion (29–32) can be brought to the bosonic form by introducing the creation operators for the mixed biexcitons:

$$B^{\dagger}_{u,\mathbf{K}} = X_{\mathbf{K}} B^{\dagger}_{\Gamma_1^+,++,\mathbf{K}} + P_{\mathbf{K}} B^{\dagger}_{\Gamma_1^+,--,\mathbf{K}},$$
$$B^{\dagger}_{l,\mathbf{K}} = -X_{\mathbf{K}} B^{\dagger}_{\Gamma_1^+,--,\mathbf{K}} + P_{\mathbf{K}} B^{\dagger}_{\Gamma_1^+,++,\mathbf{K}}.$$

Here $X_{\mathbf{K}}$ and $P_{\mathbf{K}}$ are the Hopfield coefficients, which represent the symmetric and asymmetric fraction of the biexciton in cuprous oxide:

$$|X_{\mathbf{K}}|^{-2} = 1 + \left(\frac{E\left(\Gamma^+_{5,yz}, \mathbf{K}/2\right) - E\left(\Gamma^+_{5,xz}, \mathbf{K}/2\right)}{2\left(E\left(\Gamma^+_{1,++}, \mathbf{K}\right) - E\left(\Gamma^+_{1,--}, \mathbf{K}\right)\right)} \right)^2,$$
$$|P_{\mathbf{K}}|^2 = 1 - |X_{\mathbf{K}}|^2.$$

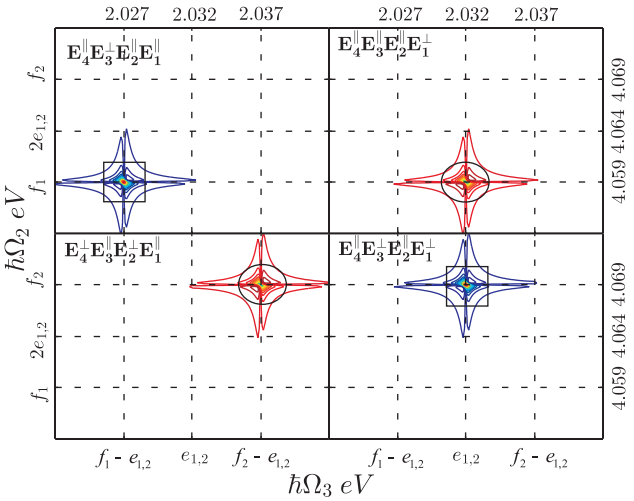

Figure 5 (online colour at: www.pss-b.com) Chirality effects along the main crystal axis allows selective absorptive or gaining non-linear response. This figure represent $\Im S^{(3)}(t_1 = 0, \Omega_2, \Omega_3)$ of 2D spectrum for $\mathbf{k}_j \| [001]$ sample orientation and $\mathbf{E}_j^{\parallel} \| [100]$, $\mathbf{E}_j^{\perp} \| [010]$. The exciton/biexciton equilibrium $n_e = n_f$ is assumed at the exciton temperature $T = 40$ K. The squares stand for the absorptive and circles stand for gaining contributions to the response function.

It is clear that the two branches are reduced to what we discussed above if the exciton degeneracy is considered.

The mixed biexciton energies are:

$$E_{u/l,\mathbf{K}} = \frac{E\left(\Gamma^+_{1,++}, \mathbf{K}\right) + E\left(\Gamma^+_{1,--}, \mathbf{K}\right)}{2} \pm \left(\left(E\left(\Gamma^+_{1,++}, \mathbf{K}\right) - E\left(\Gamma^+_{1,--}, \mathbf{K}\right)\right)^2/4 + 4\left(E\left(\Gamma^+_{5,yz}, \mathbf{K}/2\right) - E\left(\Gamma^+_{5,xz}, \mathbf{K}/2\right)\right)^2 \right)^{1/2}. \quad (18)$$

This mixing effect may be observed in a strong external magnetic field due to strong Zeeman splitting between the *ortho*-exciton levels. The above expression suggests that the biexciton resonances may be manipulated by lifting the degeneracy of the OE.

5 Conclusions We have demonstrated how 2D coherent correlation optical spectroscopy can be employed to study the optically forbidden biexciton states in cuprous oxide. Although the direct optical excitation of these dark states is not possible, the proposed non-linear optical experiment allows to measure the coherence between quadrupole-allowed 1*S* exciton manifold and the biexcitons. The biexciton binding energy may be restored by measuring the spectral distance between the cross resonances in the correlation spectra. The ellipticity and size of these resonances gives the information on the initial exciton/biexciton density distribution. Direct evidence and energies of the biexciton states are crucial for explaining the

extremely fast Auger relaxation in bulk cuprous oxide crystals. The biexciton induced Auger process heats the system and limits the exciton density at a given temperature, impeding the possible BEC of the quadrupole excitons. According to our theory the positions of the biexciton resonances are defined by the energy splitting between $\Gamma^{+}_{5;yz}$ and $\Gamma^{+}_{5;xz}$ excitons, which can be tuned by an external perturbation. We attributed this effect to the broken *ortho–para* symmetry of the cuprous oxide quadrupole excitons.

We also demonstrated exciton and biexciton chirality effects on the 2D spectrum by varying the crystal orientation and pulses polarization. These are useful for quantum computing and lasing applications. For the quantum computing application we proposed to use the two orthogonal light pulses polarizations as quantum bits. Coherence between the exciton/biexciton manifolds provides the coherent manipulation of the q-bits by focusing on different points on the 2D quadrupole spectra. That is properly polarized and timed heterodyne signals reveal the information on incoming q-bits. We illustrated this idea by describing the optical logical element OR for the given q-bits and sample orientation. Such ultrafast (fs) optical element could have interesting applications. Specific crystal orientations and pulses polarizations provide the induced negative (gaining) refractive index of the system. We, therefore, propose to utilize the corresponding exciton/biexciton coherence to induce lasing by returning the signal back to the crystal.

Appendix A: Exciton–exciton interaction in cuprous oxide In this appendix we derive the Hamiltonian specific for the quadrupole excitons in cuprous oxide, starting from the conventional Hamiltonian describing the weakly interacting bosons. In the boson representation, when the excitons are treated as structureless quasiparticles, the Hamiltonian describing the exciton–exciton interaction has the form:

$$\begin{aligned} H = &\sum_{\mathbf{k}}\sum_{i=1}^{4} E_{\mathrm{ex},i}(\mathbf{k}) a^{\dagger}_{\mathbf{k},i} a_{\mathbf{k},i} + \frac{1}{2V}\sum_{\mathbf{k}_1,\mathbf{k}_2;\mathbf{k}'_1,\mathbf{k}'_2} \delta(\mathbf{k}_1+\mathbf{k}_2,\mathbf{k}'_1+\mathbf{k}'_2) \\ &\times U_{++}(\mathbf{k}_1,\mathbf{k}_2;\mathbf{k}'_1,\mathbf{k}'_2)\left(\sum_{i=1}^{4} a^{\dagger}_{\mathbf{k}_1,i} a^{\dagger}_{\mathbf{k}_2,i} a_{\mathbf{k}'_2,i} a_{\mathbf{k}'_1,i} + 2\sum_{\substack{i=3,4\\ j=1,2}} a^{\dagger}_{\mathbf{k}_1,i} a^{\dagger}_{\mathbf{k}_2,j} a_{\mathbf{k}'_2,j} a_{\mathbf{k}'_1,i}\right) \\ &+ [U_{++}(\mathbf{k}_1,\mathbf{k}_2;\mathbf{k}'_1,\mathbf{k}'_2) + U_{--}(\mathbf{k}_1,\mathbf{k}_2;\mathbf{k}'_1,\mathbf{k}'_2)]\left(a^{\dagger}_{\mathbf{k}_1,3} a^{\dagger}_{\mathbf{k}_2,4} a_{\mathbf{k}'_2,4} a_{\mathbf{k}'_1,3} + a^{\dagger}_{\mathbf{k}_1,1} a^{\dagger}_{\mathbf{k}_2,2} a_{\mathbf{k}'_2,2} a_{\mathbf{k}'_1,1}\right) \\ &+ [U_{++}(\mathbf{k}_1,\mathbf{k}_2;\mathbf{k}'_1,\mathbf{k}'_2) - U_{--}(\mathbf{k}_1,\mathbf{k}_2;\mathbf{k}'_1,\mathbf{k}'_2)]\left(a^{\dagger}_{\mathbf{k}_1,3} a^{\dagger}_{\mathbf{k}_2,4} a_{\mathbf{k}'_2,1} a_{\mathbf{k}'_1,2} + a^{\dagger}_{\mathbf{k}_1,1} a^{\dagger}_{\mathbf{k}_2,2} a_{\mathbf{k}'_2,3} a_{\mathbf{k}'_1,4}\right). \end{aligned} \tag{19}$$

Here $E_{\mathrm{ex}}(\mathbf{k})$ is the exciton creation energy. Symmetric and asymmetric exciton–exciton interactions are denoted as $U_{\pm\pm}(\mathbf{k}_1,\mathbf{k}_2;\mathbf{k}'_1,\mathbf{k}'_2)$.

The exciton creation operators are denoted in terms of creation operators for the electron (α), hole (β) and their relative motion ($\phi(\mathbf{q})$) as:

$$a^{\dagger}_{\mathbf{k};i=1,2,3,4} = \frac{1}{\sqrt{V}}\sum_{\mathbf{q}} \phi(\mathbf{q}) \alpha^{\dagger}_{\alpha'\mathbf{k}+\mathbf{q},\sigma_1} \beta^{\dagger}_{\beta'\mathbf{k}-\mathbf{q},\sigma_2}. \tag{20}$$

Here $\alpha' = m_{\mathrm{e}}/m_{\mathrm{ex}}$, $\beta' = m_{\mathrm{h}}/m_{\mathrm{ex}}$ and the net spin indexes are:

$i = 1 \rightarrow (\sigma_1 = 1/2,\ \sigma_2 = 1/2)$,
$i = 2 \rightarrow (\sigma_1 = -1/2,\ \sigma_2 = -1/2)$,
$i = 3 \rightarrow (\sigma_1 = 1/2,\ \sigma_2 = -1/2)$,
$i = 4 \rightarrow (\sigma_1 = -1/2,\ \sigma_2 = 1/2)$.

The wave functions of the Γ^{+}_{2} and ${}^{3}\Gamma^{+}_{5}$ excitons are written as [30]:

$$\left|\Gamma^{+}_{5,yz;\mathbf{k}}\right\rangle = -\frac{i}{\sqrt{2V}}\sum_{\mathbf{q}} \phi(\mathbf{q})\left(\alpha^{\dagger}_{\alpha'\mathbf{k}+\mathbf{q},1/2}\beta^{\dagger}_{\beta'\mathbf{k}-\mathbf{q},-1/2} + \alpha^{\dagger}_{\alpha'\mathbf{k}+\mathbf{q},-1/2}\beta^{\dagger}_{\beta'\mathbf{k}-\mathbf{q},1/2}\right)|0\rangle, \tag{21}$$

$$\left|\Gamma^{+}_{5,xz;\mathbf{k}}\right\rangle = \frac{1}{\sqrt{2V}}\sum_{\mathbf{q}} \phi(\mathbf{q})\left(\alpha^{\dagger}_{\alpha'\mathbf{k}+\mathbf{q},-1/2}\beta^{\dagger}_{\beta'\mathbf{k}-\mathbf{q},1/2} - \alpha^{\dagger}_{\alpha'\mathbf{k}+\mathbf{q},1/2}\beta^{\dagger}_{\beta'\mathbf{k}-\mathbf{q},-1/2}\right)|0\rangle, \tag{22}$$

$$\left|\Gamma^{+}_{5,xy;\mathbf{k}}\right\rangle = -\frac{i}{\sqrt{2V}}\sum_{\mathbf{q}} \phi(\mathbf{q})\left(\alpha^{\dagger}_{\alpha'\mathbf{k}+\mathbf{q},1/2}\beta^{\dagger}_{\beta'\mathbf{k}-\mathbf{q},1/2} - \alpha^{\dagger}_{\alpha'\mathbf{k}+\mathbf{q},-1/2}\beta^{\dagger}_{\beta'\mathbf{k}-\mathbf{q},-1/2}\right)|0\rangle, \tag{23}$$

$$\left|\Gamma^{+}_{2;\mathbf{k}}\right\rangle = \frac{1}{\sqrt{2V}}\sum_{\mathbf{q}}\phi(\mathbf{q})\left(\alpha^{\dagger}_{\alpha'\mathbf{k}+\mathbf{q},1/2}\beta^{\dagger}_{\beta'\mathbf{k}-\mathbf{q},1/2}+\alpha^{\dagger}_{\alpha'\mathbf{k}+\mathbf{q},-1/2}\beta^{\dagger}_{\beta'\mathbf{k}-\mathbf{q},-1/2}\right)|0\rangle. \tag{24}$$

Therefore from (20), the creation operators for the Γ_2^+ and ${}^3\Gamma_5^+$ excitons have the following form:

$$\begin{aligned}
b^{\dagger}_{\Gamma^{+}_{5,yz};\mathbf{k}} &= b^{\dagger}_{\mathbf{k},1} = -\frac{i}{\sqrt{2}}\left(a^{\dagger}_{\mathbf{k},3}+a^{\dagger}_{\mathbf{k},4}\right) = -i\alpha^{\dagger}_{\mathbf{k},\Gamma_2,4}; \qquad a^{\dagger}_{\mathbf{k},1} = \frac{1}{\sqrt{2}}\left(b^{\dagger}_{\mathbf{k},4}+ib^{\dagger}_{\mathbf{k},3}\right)\\
b^{\dagger}_{\Gamma^{+}_{5,xz};\mathbf{k}} &= b^{\dagger}_{\mathbf{k},2} = \frac{1}{\sqrt{2}}\left(a^{\dagger}_{\mathbf{k},4}-a^{\dagger}_{\mathbf{k},3}\right) = -\alpha^{\dagger}_{\mathbf{k},\Gamma_{5,z},3}; \qquad a^{\dagger}_{\mathbf{k},2} = \frac{1}{\sqrt{2}}\left(b^{\dagger}_{\mathbf{k},4}-ib^{\dagger}_{\mathbf{k},3}\right)\\
b^{\dagger}_{\Gamma^{+}_{5,xy};\mathbf{k}} &= b^{\dagger}_{\mathbf{k},3} = -\frac{i}{\sqrt{2}}\left(a^{\dagger}_{\mathbf{k},1}-a^{\dagger}_{\mathbf{k},2}\right) = -i\alpha^{\dagger}_{\mathbf{k},\Gamma_{5,y},2}; \qquad a^{\dagger}_{\mathbf{k},3} = -\frac{1}{\sqrt{2}}\left(b^{\dagger}_{\mathbf{k},2}-ib^{\dagger}_{\mathbf{k},1}\right)\\
b^{\dagger}_{\Gamma^{+}_{2;\mathbf{k}}} &= b^{\dagger}_{\mathbf{k},4} = \frac{1}{\sqrt{2}}\left(a^{\dagger}_{\mathbf{k},1}+a^{\dagger}_{\mathbf{k},2}\right) = \alpha^{\dagger}_{\mathbf{k},\Gamma_{5,x},1}; \qquad a^{\dagger}_{\mathbf{k},4} = \frac{1}{\sqrt{2}}\left(b^{\dagger}_{\mathbf{k},2}+ib^{\dagger}_{\mathbf{k},1}\right).
\end{aligned} \tag{25}$$

Above we also listed creation operators $\alpha_{\Gamma_{5,2};x,y,z}$ for the T_{d} group (CuCl-for example [16], page 149). Using the transformations (25) along with the bosonic Hamiltonian (19) one gets the cuprous oxide Hamiltonian.

Appendix B In this appendix we derive equation of motion for the exciton and lowest biexciton state for the pulses scheme known as k_{III} technique. The equations of motion for one and two exciton state can be written as following:

$$\begin{aligned}
i\hbar\frac{\mathrm{d}}{\mathrm{d}t}\left\langle b^{\dagger}_{\mathbf{k},1}\right\rangle &= E\left(\Gamma^{+}_{5,yz},\mathbf{k}\right)\left\langle b^{\dagger}_{\mathbf{k},1}\right\rangle + \frac{1}{4V}\sum_{\mathbf{p},\mathbf{q}}[U_{--}-U_{++}]\left\langle b^{\dagger}_{\mathbf{p},2}b^{\dagger}_{\mathbf{q},2}b_{\mathbf{p}+\mathbf{q}-\mathbf{k},1}\right\rangle + \sum_{j=1}^{4}\delta_{\mathbf{k},\mathbf{k}_j}\mathbf{E}_j(\mathbf{k},t)\mathbf{d}_1(\mathbf{k},\mathbf{E}/E),\\
i\hbar\frac{\mathrm{d}}{\mathrm{d}t}\left\langle b^{\dagger}_{\mathbf{k},2}\right\rangle &= E\left(\Gamma^{+}_{5,xz},\mathbf{k}\right)\left\langle b^{\dagger}_{\mathbf{k},2}\right\rangle + \frac{1}{4V}\sum_{\mathbf{p},\mathbf{q}}[U_{--}-U_{++}]\left\langle b^{\dagger}_{\mathbf{p},1}b^{\dagger}_{\mathbf{q},1}b_{\mathbf{p}+\mathbf{q}-\mathbf{k},2}\right\rangle + \sum_{j=1}^{4}\delta_{\mathbf{k},\mathbf{k}_j}\mathbf{E}_j(\mathbf{k},t)\mathbf{d}_2(\mathbf{k},\mathbf{E}/E),\\
i\hbar\frac{\mathrm{d}}{\mathrm{d}t}\left\langle b^{\dagger}_{\mathbf{p},1}b^{\dagger}_{\mathbf{q},1}\right\rangle &= \left(E\left(\Gamma^{+}_{5,yz},\mathbf{p}\right)+E\left(\Gamma^{+}_{5,yz},\mathbf{q}\right)\right)\left\langle b^{\dagger}_{\mathbf{p},1}b^{\dagger}_{\mathbf{q},1}\right\rangle\\
&\quad+\frac{1}{4V}\sum_{\mathbf{p}',\mathbf{q}'}[U_{--}-U_{++}]\left\langle b^{\dagger}_{\mathbf{p}',2}b^{\dagger}_{\mathbf{q}',2}\right\rangle\left(\delta_{\mathbf{q}'+\mathbf{p}'-\mathbf{p},\mathbf{q}}+\left\langle b^{\dagger}_{\mathbf{q},1}b_{\mathbf{p}'+\mathbf{q}'-\mathbf{p},1}\right\rangle+\left\langle b^{\dagger}_{\mathbf{p},1}b_{\mathbf{q}'+\mathbf{p}'-\mathbf{q},1}\right\rangle\right)\\
&\quad-\sum_{j=1}^{4}\delta_{\mathbf{q},\mathbf{k}_j}\mathbf{E}_j(\mathbf{q},t)\mathbf{d}_1(\mathbf{q},\mathbf{E}/E)\left\langle b^{\dagger}_{1,\mathbf{q}}\right\rangle-\sum_{j=1}^{4}\delta_{\mathbf{p},\mathbf{k}_j}\mathbf{E}_j(\mathbf{p},t)\mathbf{d}_1(\mathbf{p},\mathbf{E}/E)\left\langle b^{\dagger}_{1,\mathbf{p}}\right\rangle,\\
i\hbar\frac{\mathrm{d}}{\mathrm{d}t}\left\langle b^{\dagger}_{\mathbf{p},2}b^{\dagger}_{\mathbf{q},2}\right\rangle &= \left(E\left(\Gamma^{+}_{5,xz},\mathbf{p}\right)+E\left(\Gamma^{+}_{5,xz},\mathbf{q}\right)\right)\left\langle b^{\dagger}_{\mathbf{p},2}b^{\dagger}_{\mathbf{q},2}\right\rangle\\
&\quad+\frac{1}{4V}\sum_{\mathbf{p}',\mathbf{q}'}[U_{--}-U_{++}]\left\langle b^{\dagger}_{\mathbf{p}',1}b^{\dagger}_{\mathbf{q}',1}\right\rangle\left(\delta_{\mathbf{q}'+\mathbf{p}'-\mathbf{p},\mathbf{q}}+\left\langle b^{\dagger}_{\mathbf{q},2}b_{\mathbf{p}'+\mathbf{q}'-\mathbf{p},2}\right\rangle+\left\langle b^{\dagger}_{\mathbf{p},2}b_{\mathbf{q}'+\mathbf{p}'-\mathbf{q},2}\right\rangle\right)\\
&\quad-\sum_{j=1}^{4}\delta_{\mathbf{q},\mathbf{k}_j}\mathbf{E}_j(\mathbf{q},t)\mathbf{d}_2(\mathbf{q},\mathbf{E}/E)\left\langle b^{\dagger}_{2,\mathbf{q}}\right\rangle-\sum_{j=1}^{4}\delta_{\mathbf{p},\mathbf{k}_j}\mathbf{E}_j(\mathbf{k},t)\mathbf{d}_2(\mathbf{p},\mathbf{E}/E)\left\langle b^{\dagger}_{2,\mathbf{p}}\right\rangle.
\end{aligned} \tag{26}$$

Due to the normal ordering of the operators, one can perform the factorization in the center of mass of the biexciton momenta $\mathbf{K}$ as following:

$$\sum_{\mathbf{p},\mathbf{q}}\left\langle b^{\dagger}_{\mathbf{p},i}b^{\dagger}_{\mathbf{q},i}b^{\dagger}_{\mathbf{p}+\mathbf{q}-\mathbf{k},j\neq i}\right\rangle = \sum_{\mathbf{l},\mathbf{K}}\left\langle b^{\dagger}_{\mathbf{l}+\mathbf{K}/2,i}b^{\dagger}_{-\mathbf{l}+\mathbf{K}/2,i}\right\rangle\left\langle b^{\dagger}_{\mathbf{K}-\mathbf{k},j\neq i}\right\rangle. \tag{27}$$

Using the orthogonality conditions:

$$\begin{aligned}
\frac{1}{V}\sum_{\mathbf{l}}\Psi^{*}_{J,\mathbf{l}}\Psi_{J',\mathbf{l}} &= \delta_{J,J'}\\
\frac{1}{V}\sum_{J}\Psi^{*}_{J,\mathbf{l}}\Psi_{J,\mathbf{l}'} &= \delta_{\mathbf{l},\mathbf{l}'},
\end{aligned}$$

and keeping the resonant term $J=1S$ only, one has:

$$\left\langle b^{\dagger}_{\mathbf{l}+\mathbf{K}/2,i} b^{\dagger}_{-\mathbf{l}+\mathbf{K}/2,i} \right\rangle = \frac{1}{\sqrt{V}} \Psi^{*}_{1S,\mathbf{l}} \left(B^{\dagger}_{\mathbf{K},\Gamma^{+}_{1,++}} \pm B^{\dagger}_{\mathbf{K},\Gamma^{+}_{1,--}} \right). \tag{28}$$

For the low density excitation limit one can simplify the last two equations in the system (26) using the following identity:

$$\sum_{\mathbf{p}',\mathbf{q}'} \left\langle b^{\dagger}_{\mathbf{p}',i} b^{\dagger}_{\mathbf{q}',i} \right\rangle \left(\delta_{\mathbf{q}'+\mathbf{p}'-\mathbf{p},\mathbf{q}} + \delta_{\mathbf{q}'+\mathbf{p}'+\mathbf{q},\mathbf{p}} + \left\langle b^{\dagger}_{\mathbf{q},j\neq i} b_{\mathbf{p}'+\mathbf{q}'-\mathbf{p},j\neq i} \right\rangle + \left\langle b^{\dagger}_{\mathbf{p},j\neq i} b_{\mathbf{q}'+\mathbf{p}'+\mathbf{q},j\neq i} \right\rangle \right) \approx \sum_{\mathbf{l}',\mathbf{K}'/2} \delta_{\mathbf{K},\mathbf{K}'} \left\langle b^{\dagger}_{\mathbf{l}'+\mathbf{K}'/2,i} b^{\dagger}_{-\mathbf{l}'+\mathbf{K}'/2,i} \right\rangle.$$

Putting Eqs. (27,28) into (26) one gets the equations of motion for the exciton and biexciton variables for the *weakly interacting* bosons model:

$$\begin{aligned} i\hbar \frac{\mathrm{d}}{\mathrm{d}t} \left\langle b^{\dagger}_{\mathbf{k},1} \right\rangle &= E\left(\Gamma^{+}_{5,yz},\mathbf{k}\right) \left\langle b^{\dagger}_{\mathbf{k},1} \right\rangle + \frac{1}{4V} \sum_{\mathbf{l},\mathbf{K}} [U_{--} - U_{++}] \frac{\Psi^{*}_{\Gamma^{+}_{1},\mathbf{l}}}{\sqrt{V}} \left(\left\langle B^{\dagger}_{\mathbf{K},\Gamma^{+}_{1,++}} \right\rangle - \left\langle B^{\dagger}_{\mathbf{K},\Gamma^{+}_{1,--}} \right\rangle \right) \langle b_{\mathbf{K}-\mathbf{k},1} \rangle \\ &\quad - \sum_{j=1}^{4} \delta_{\mathbf{k},\mathbf{k}_j} \mathbf{E}_j(\mathbf{k},t) \mathbf{d}_1(\mathbf{k},\mathbf{E}/E), \end{aligned} \tag{29}$$

$$\begin{aligned} i\hbar \frac{\mathrm{d}}{\mathrm{d}t} \left\langle b^{\dagger}_{\mathbf{k},2} \right\rangle &= E\left(\Gamma^{+}_{5,xz},\mathbf{k}\right) \left\langle b^{\dagger}_{\mathbf{k},2} \right\rangle + \frac{1}{4V} \sum_{\mathbf{l},\mathbf{K}} [U_{--} - U_{++}] \frac{\Psi^{*}_{\Gamma^{+}_{1},\mathbf{l}}}{\sqrt{V}} \left(\left\langle B^{\dagger}_{\mathbf{K},\Gamma^{+}_{1,++}} \right\rangle + \left\langle B^{\dagger}_{\mathbf{K},\Gamma^{+}_{1,--}} \right\rangle \right) \langle b_{\mathbf{K}-\mathbf{k},2} \rangle \\ &\quad - \sum_{j=1}^{4} \delta_{\mathbf{k},\mathbf{k}_j} \mathbf{E}_j(\mathbf{k},t) \mathbf{d}_2(\mathbf{k},\mathbf{E}/E), \end{aligned} \tag{30}$$

$$\begin{aligned} i\hbar \frac{\mathrm{d}}{\mathrm{d}t} \left\langle B^{\dagger}_{\mathbf{K},\Gamma^{+}_{1,++}} \right\rangle &= \left(E\left(\Gamma^{+}_{5,yz,\mathbf{K}/2}\right) + E\left(\Gamma^{+}_{5,xz,\mathbf{K}/2}\right) \right) \left\langle B^{\dagger}_{\mathbf{K},\Gamma^{+}_{1,++}} \right\rangle + \left(E\left(\Gamma^{+}_{5,yz,\mathbf{K}/2}\right) - E\left(\Gamma^{+}_{5,xz,\mathbf{K}/2}\right) \right) \left\langle B^{\dagger}_{\mathbf{K},\Gamma^{+}_{1,--}} \right\rangle \\ &\quad - \frac{1}{4V^2} \sum_{\mathbf{l},\mathbf{l}'} [U_{--} - U_{++}] \Psi^{*}_{\Gamma^{+}_{1},\mathbf{l}'} \Psi_{\Gamma^{+}_{1},\mathbf{l}} \left\langle B^{\dagger}_{\mathbf{K},\Gamma^{+}_{1,++}} \right\rangle \\ &\quad - \frac{1}{2\sqrt{V}} \sum_{j=1}^{4} \mathbf{E}_j(\mathbf{k}_j,t) \left(\Psi_{\Gamma^{+}_{1},\mathbf{K}/2-\mathbf{k}_j} + \Psi_{\Gamma^{+}_{1},\mathbf{k}_j-\mathbf{K}/2} \right) \left(\mathbf{d}_1(\mathbf{k}_j,\mathbf{E}/E) \left\langle b^{\dagger}_{\mathbf{k}_j,1} \right\rangle - \mathbf{d}_2(\mathbf{k}_j,\mathbf{E}/E) \left\langle b^{\dagger}_{\mathbf{k}_j,2} \right\rangle \right), \end{aligned} \tag{31}$$

$$\begin{aligned} i\hbar \frac{\mathrm{d}}{\mathrm{d}t} \left\langle B^{\dagger}_{\mathbf{K},\Gamma^{+}_{1,--}} \right\rangle &= \left(E\left(\Gamma^{+}_{5,yz,\mathbf{K}/2}\right) + E\left(\Gamma^{+}_{5,xz,\mathbf{K}/2}\right) \right) \left\langle B^{\dagger}_{\mathbf{K},\Gamma^{+}_{1,--}} \right\rangle \\ &\quad + \left(E\left(\Gamma^{+}_{5,yz,\mathbf{K}/2}\right) - E\left(\Gamma^{+}_{5,xz,\mathbf{K}/2}\right) \right) \left\langle B^{\dagger}_{\mathbf{K},\Gamma^{+}_{1,++}} \right\rangle + \frac{1}{4V^2} \sum_{\mathbf{l},\mathbf{l}'} [U_{--} - U_{++}] \Psi^{*}_{\Gamma^{+}_{1},\mathbf{l}'} \Psi_{\Gamma^{+}_{1},\mathbf{l}} \left\langle B^{\dagger}_{\mathbf{K},\Gamma^{+}_{1,--}} \right\rangle \\ &\quad - \frac{1}{2\sqrt{V}} \sum_{j=1}^{4} \mathbf{E}_j(\mathbf{k}_j,t) \left(\Psi_{\Gamma^{+}_{1},\mathbf{K}/2-\mathbf{k}_j} + \Psi_{\Gamma^{+}_{1},\mathbf{k}_j-\mathbf{K}/2} \right) \left(\mathbf{d}_1(\mathbf{k}_j,\mathbf{E}/E) \left\langle b^{\dagger}_{\mathbf{k}_j,1} \right\rangle + \mathbf{d}_2(\mathbf{k}_j,\mathbf{E}/E) \left\langle b^{\dagger}_{\mathbf{k}_j,2} \right\rangle \right). \end{aligned} \tag{32}$$

The corresponding equations of motions within the *independent* boson model are listed below:

$$\begin{aligned} i\hbar \frac{\mathrm{d}}{\mathrm{d}t} \left\langle b^{\dagger}_{\mathbf{k},1} \right\rangle &= E\left(\Gamma^{+}_{5,yz},\mathbf{k}\right) \left\langle b^{\dagger}_{\mathbf{k},1} \right\rangle + \sum_{\mathbf{K},\mathbf{k}_j,j}^{4} \mathbf{E}_j \left(\mathbf{D}^{++}_{1}(\mathbf{K},\mathbf{k}_j) \left\langle B^{\dagger}_{\mathbf{K},\Gamma^{+}_{1,++}} \right\rangle + \mathbf{D}^{--}_{1}(\mathbf{K},\mathbf{k}_j) \left\langle B^{\dagger}_{\mathbf{K},\Gamma^{+}_{1,--}} \right\rangle \right) \\ &\quad - \sum_{j=1}^{4} \delta_{\mathbf{k},\mathbf{k}_j} \mathbf{E}_j(\mathbf{k},t) \mathbf{d}_1(\mathbf{k},\mathbf{E}/E), \end{aligned} \tag{33}$$

$$\begin{aligned} i\hbar \frac{\mathrm{d}}{\mathrm{d}t} \left\langle b^{\dagger}_{\mathbf{k},2} \right\rangle &= E\left(\Gamma^{+}_{5,xz},\mathbf{k}\right) \left\langle b^{\dagger}_{\mathbf{k},2} \right\rangle + \sum_{\mathbf{K},\mathbf{k}_j,j}^{4} \mathbf{E}_j \left(\mathbf{D}^{++}_{2}(\mathbf{K},\mathbf{k}_j) \left\langle B^{\dagger}_{\mathbf{K},\Gamma^{+}_{1,++}} \right\rangle + \mathbf{D}^{--}_{2}(\mathbf{K},\mathbf{k}_j) \left\langle B^{\dagger}_{\mathbf{K},\Gamma^{+}_{1,--}} \right\rangle \right) \\ &\quad - \sum_{j=1}^{4} \delta_{\mathbf{k},\mathbf{k}_j} \mathbf{E}_j(\mathbf{k},t) \mathbf{d}_2(\mathbf{k},\mathbf{E}/E), \end{aligned} \tag{34}$$

$$i\hbar\frac{\mathrm{d}}{\mathrm{d}t}\left\langle B^{\dagger}_{\mathbf{K},\Gamma^{+}_{1,++}}\right\rangle = E\left(\Gamma^{+}_{1,++,\mathbf{K}}\right)\left\langle B^{\dagger}_{\mathbf{K},\Gamma^{+}_{1,++}}\right\rangle - \sum_{\mathbf{K},j}^{4}\mathbf{E}_j\left(\mathbf{D}_1^{++}(\mathbf{K},\mathbf{k}_j)\left\langle b^{\dagger}_{\mathbf{k},1}\right\rangle - \mathbf{D}_2^{++}(\mathbf{K},\mathbf{k}_j)\left\langle b^{\dagger}_{\mathbf{k},2}\right\rangle\right), \tag{35}$$

$$i\hbar\frac{\mathrm{d}}{\mathrm{d}t}\left\langle B^{\dagger}_{\mathbf{K},\Gamma^{+}_{1,--}}\right\rangle = E\left(\Gamma^{+}_{1,--,\mathbf{K}}\right)\left\langle B^{\dagger}_{\mathbf{K},\Gamma^{+}_{1,--}}\right\rangle - \sum_{\mathbf{K},j}^{4}\mathbf{E}\left(\mathbf{D}_1^{--}(\mathbf{K},\mathbf{k}_j)\left\langle b^{\dagger}_{\mathbf{k},1}\right\rangle + \mathbf{D}_2^{--}(\mathbf{K},\mathbf{k}_j)\left\langle b^{\dagger}_{\mathbf{k},2}\right\rangle\right). \tag{36}$$

Acknowledgements This work was supported by the National Institutes of Health Grant GM59230 and National Science Foundation Grant CHE-0446555, and by a CUNY-PSC-FRAP Grant.

References

[1] G. M. Kavoulakis, Y.-C. Chang, and G. Baym, Phys. Rev. B **55**, 7593 (1997).
[2] K. E. O'Hara, J. R. Gullingsrud, and J. P. Wolfe, Phys. Rev. B **60**, 10872 (1999).
[3] J. T. Warren, K. E. O'Hara, and J. P. Wolfe, Phys. Rev. B **61**, 8215 (2000).
[4] D. W. Snoke and V. Negoita, Phys. Rev. B **61**, 2904 (2000).
[5] K. E. O'Hara and J. P. Wolfe, Phys. Rev. B **62**, 12909 (2000).
[6] S. Denev and D. W. Snoke, Phys. Rev. B **65**, 085211 (2002).
[7] J. Jang and J. Wolfe, Solid State Commun. **137**, 91 (2006a).
[8] G. Kavoulakis and G. Baym, Phys. Rev. B **54**, 16625 (1996).
[9] G. Kavoulakis, G. Baym, and J. Wolfe, Phys. Rev. B **53**, 7227 (1996).
[10] J. I. Jang and J. P. Wolfe, Phys. Rev. B **74**, 045211 (2006b).
[11] X. Li, T. Zhang, C. N. Borca, and S. T. Cundiff, Phys. Rev. Lett. **96**, 057406 (2006).
[12] S. Adachi, K. Hazu, T. Sota, S. Chichibu, G. Cantwell, D. Eason, D. Reynolds, and C. Litton, Semicond. Sci. Technol. **19**, S276 (2004).
[13] E. Finger, S. Kraft, M. Hofmann, T. Meier, and S. Koch, Phys. Status Solidi B **234**, 424 (2002).
[14] L. Yang and S. Mukamel, Phys. Rev. Lett. **100**, 057402 (2008).
[15] D. Fröhlich, G. Dasbach, G. Baldassarri Höger von Högersthal, M. Bayer, R. Klieber, D. Suter, and H. Stolz, Solid State Commun. **134**, 139 (2005).
[16] S. Moskalenko and D. Snoke, Bose–Einstein Condensation of Excitons and Biexcitons (Cambridge University Press, New York, 2000).
[17] J. Forney, Nuovo Cimento B **22**, 153 (1974).
[18] A. Bobrysheva and S. Moskalenko, Phys. Status Solidi B **119**, 141 (1983).
[19] D. Abramavicius, W. Zhuang, and S. Mukamel, J. Phys. B, Atom. Mol. Opt. Phys. **39**, 5051 (2006).
[20] R. Ernst, G. Bodenhausen, and A. Wokaun, Principles of Nuclear Magnetic Resonance in One and Two Dimensions (Oxford University Press, New York, 1990).
[21] S. Mukamel, Annu. Rev. Phys. Chem. **51**, 691 (2000).
[22] T. Brixner, J. Stenger, H. Vaswani, M. Cho, R. Blankenship, and G. Fleming, Nature **434**, 625 (2005).
[23] M. Asplund, M. Zanni, and R. Hochstrasser, Proc. Natl. Acad. Sci. USA **97**, 8219 (2000).
[24] L. Yang, I. Schweigert, S. Cundiff, and S. Mukamel, Phys. Rev. B **75**, 125302 (2007).
[25] M. Erementchouk, M. N. Leuenberger, and L. J. Sham, Phys. Rev. B **76**, 115307 (2007).
[26] I. Kuznetsova, P. Thomas, T. Meier, T. Zhang, X. Li, R. Mirin, and S. Cundiff, Solid State Commun. **142**, 154 (2007).
[27] A. L. Ivanov and H. Haug, Phys. Rev. B **48**, 1490 (1993).
[28] S. Mukamel, R. Oszwaldowski, and D. Abramavicius, Phys. Rev. B **75**, 245305 (2007).
[29] A. I. Bobrysheva, M. F. Miglei, and M. I. Shmiglyuk, Phys. Status Solidi B **53**, 71 (1972).
[30] S. Moskalenko, A. Bobrysheva, and E. Kiselyova, Phys. Status Solidi B **213**, 377 (1999).
[31] W. F. Brinkman and T. M. Rice, Phys. Rev. B **8**, 1570 (1973).
[32] W. T. Huang, Phys. Status Solidi B **60**, 309 (1973).
[33] A. D. Bristow, D. Kiselyova, D. Xingcan, R. P. Mirin, and S. T. Cundiff, Phys. Rev. B **79**, 161305 (2009).